ELSEVIER

Journal of Atmospheric and Solar-Terrestrial Physics 68 (2006) 539–557

Journal of ATMOSPHERIC AND SOLAR-TERRESTRIAL PHYSICS

www.elsevier.com/locate/jastp

Ionogram height–time–intensity observations of descending sporadic *E* layers at mid-latitude

C. Haldoupis[a,*], C. Meek[b], N. Christakis[c], D. Pancheva[d], A. Bourdillon[e]

[a]*Physics Department, University of Crete, Heraklion, 710 03 Crete, Greece*
[b]*Institute of Space and Atmospheric Studies, University of Saskatchewan, Canada*
[c]*Department of Applied Mathematics, University of Crete, Greece*
[d]*Department of Electronics and Electrical Engineering, University of Bath, UK*
[e]*IETR/CNRS, Université de Rennes 1, France*

Available online 24 October 2005

Abstract

A new methodology of ionosonde height–time–intensity (HTI) analysis is introduced which allows the investigation of sporadic *E* layer (E_s) vertical motion and variability. This technique, which is useful in measuring descent rates and tidal periodicities of E_s, is applied on ionogram recordings made during a summer period from solstice to equinox on the island of Milos (36.7°N; 24.5°E). On the average, the ionogram HTI analysis revealed a pronounced semidiurnal periodicity in layer descent and occurrence. It is characterized by a daytime layer starting at 120 km near 06 h local time (LT) and moving downward to altitudes below 100 km by about 18 h LT when a nighttime layer appears above at ~125 km. The latter moves also downward but at higher descent rates (1.6–2.2 km/h) than the daytime layer (0.8–1.5 km/h). The nighttime E_s is weaker in terms of critical sporadic *E* frequencies (*foEs*), has a shorter duration, and tends to occur less during times close to solstice. Here, a diurnal periodicity in E_s becomes dominant. The HTI plots often show the daytime and nighttime E_s connecting with weak traces in the upper *E* region which occur with a semidiurnal, and at times terdiurnal, periodicity. These, which are identified as upper *E* region descending intermediate layers (DIL), play an important role in initiating and reinforcing the sporadic *E* layers below 120–125 km. The observations are interpreted by considering the downward propagation of wind shear convergent nodes that associate with the $S_{2,3}$ semidiurnal tide in the upper *E* region and the $S_{1,1}$ diurnal tide in the lower *E* region. The daytime sporadic *E* layer is attributed to the confluence of semidiurnal and diurnal convergent nodes, which may explain the well-known pre-noon daily maximum observed in *foEs*. The nighttime layer is not well understood, although most likely it is associated with the intrusion of the daytime DIL into the lower *E* region due to vertical wind shear convergence nodes descending with the semidiurnal tide. It was also found that the descent rates of sporadic *E* may not always represent the vertical phase velocities of the tides, especially in the nighttime layers. Finally, the ionosonde HTI analysis is a promising new tool for exploring long-duration data sets from ionosondes around the globe to obtain preliminary climatological studies of neutral wind dynamics at *E* region heights in the lower thermosphere.

Keywords: Sporadic *E* layers; Ionogram HTI plots; Descending layers; Atmospheric tides

*Corresponding author. Tel.: +30 2810 394222; fax: +30 2810 394201.
E-mail address: chald@physics.uoc.gr (C. Haldoupis).

1364-6826/$ - see front matter © 2005 Elsevier Ltd. All rights reserved.
doi:10.1016/j.jastp.2005.03.020

1. Introduction

The mid-latitude sporadic E layers (E_s), which are thin layers of metallic ion plasma that form at E region heights between 95 and 125 km, have been studied extensively over many years, e.g., see comprehensive reviews by Whitehead (1989) and Mathews (1998). The physics of E_s formation is based on the "wind shear" theory, in which vertical shears in the horizontal neutral wind can cause, by the combined action of ion-neutral collisional coupling and geomagnetic Lorentz forcing, the long-lived metallic ions to move vertically and converge into thin and dense plasma layers. The process is governed by ion dynamics, with the magnetized electrons only following the ions to maintain charge neutrality. In its simplest form, when diffusion and electric field forces are neglected, the wind shear theory predicts for the vertical ion drift velocity w at steady state:

$$w = \frac{\cos I \sin I}{1 + (\nu_i/\omega_i)^2} U + \frac{(\nu_i/\omega_i)\cos I}{1 + (\nu_i/\omega_i)^2} V. \quad (1)$$

Here, the notations of Mathews and Bekeny (1979) are used, in which U and V are the geomagnetic southward and eastward components of the neutral wind (representing approximately the meridional and zonal wind components, respectively), I is the magnetic dip angle, and $(\nu_i/\omega_i) = r$ is the ratio of ion-neutral collision frequency to ion gyrofrequency. Since the vertical plasma drift becomes collision-dominated below about 125 km where $r^2 \gg 1$, the wind shear mechanism requires for the formation of a layer vertical shears of a proper polarity in the zonal and meridional wind, in accord with Eq. (1).

Since most E_s are situated below about 120 km, they are controlled by vertical zonal wind shears which are characterized (for the northern hemisphere) by a westward wind above and an eastward, or smaller westward, wind below. Also, E_s are known to descend regularly with time down below 100 km where they eventually disappear, apparently because the metallic ion recombination rates become increasingly effective. On the other hand, the vertical meridional wind shears, with a northward wind above and a southward, or smaller northward, wind below, are effective in the upper E region, where they can generate, together with vertical shears in the zonal wind, the so called "descending intermediate layers" (DILs). These are weak plasma layers that initiate at the bottom of the F region and move downward, often merging with the sporadic E layers below. DILs are considered to be part of the sporadic E layer system because they appear to participate in a parenting-like process for E_s by steadily transporting metallic ions down to lower E region heights (e.g., see Fujitaka and Tohmatsu, 1973; Mathews, 1998).

Incoherent scatter radar (ISR) studies and ionosonde observations show that mid-latitude sporadic E is not as 'sporadic' as its name implies but a regularly occurring phenomenon. The repeatability in E_s layer occurrence and altitude descent are attributed to the global system of the diurnal and semidiurnal tides in the lower thermosphere. As summarized by Mathews (1998), the Arecibo ISR observations revealed a fundamental role played by the diurnal and semidiurnal tides in the formation and descent of sporadic E layers, which often are also referred to as "tidal ion layers" (TILs). The 12 and 24 h tidal effects on E_s formation have been recognized also in ionosonde observations, e.g., see MacDougall (1974), Wilkinson et al. (1992), and Szuszczewicz et al. (1995). The connection between E_s and tides is not so surprising given that the dominant winds in the E region are the solar tides (Chapman and Lindzen, 1970).

Although there exists an understanding of the tidal variability of descending mid-latitude sporadic E layers, still there are unresolved complexities in this process which require further study. For example, a point of uncertainty relates to the role and importance of the semidiurnal tides on the direct formation and descent of E_s. Important questions also exist with respect to the confluence of the various tidal modes and what do the descent rates signify. Moreover, there are questions about the tidal effects on basic E_s properties, such as the diurnal and seasonal variability of the layers, which are still not well understood.

The purpose of the present work is to provide more insight into the topic of sporadic E tidal variability and layer descent by means of using a novel method for the presentation of the ionosonde data. In this method, ionograms are used to construct height–time–intensity (HTI) plots for one or more ionosonde frequency bins. This presentation, which was developed for the analysis of Canadian advanced digital ionosonde (CADI) data, turned out to be quite suitable for studying sporadic E layer dynamics and height variability. Also, and in relation to the powerful ISR technique, the HTI methodology can be supplementary

because an ionosonde has the advantage of making long-term measurements which are necessary for studying tidal and planetary wave effects on ionospheric plasma (e.g., see Haldoupis and Pancheva, 2002; Pancheva et al., 2003; Haldoupis et al., 2004).

In the following we first introduce the ionosonde HTI method which is applied here on high-time resolution ionograms. Next, the analysis focuses on finding the average tidal variations and descent rates of sporadic E layers during a 3-month period extending from the summer solstice to equinox. The findings are first presented and then compared to the Arecibo ISR observations. Then, the physical picture that emerges from the present and past knowledge is presented, followed by a numerical simulation based on the wind shear theory. Finally, the paper closes with a summary of the main results and a few concluding comments.

2. Ionogram height–time–intensity analysis

We introduce a new presentation of the ionosonde observations which relies on the concept of range-time intensity (RTI) plots of a single frequency radar. Given that the ionogram represents a "snapshot" of the reflected signal power as a function of (virtual) height and radio frequency, one would select any frequency bin and use sequential ionograms to compute the reflected power as a function of height and time, and thus obtain a HTI display. The HTI plot has the merits of the common RTI radar plot which can monitor dynamic changes in the medium. In producing an HTI plot, the choice of the ionosonde frequency is important because it relates to the ionospheric electron density at the reflection height, i.e., $f \propto \sqrt{N_e}$. For example, in order to observe daytime F region changes, a frequency must be selected which is higher than the critical E region frequency foE. Also, in order to minimize the height uncertainties, the HTI frequency cannot be near the E and F layer critical frequencies, otherwise the measured virtual heights can differ from the real heights significantly.

The software developed for the analysis allows first the selection of several, overlapping or not, ionosonde frequency bins of equal or different extent, and then computes the corresponding HTI plots within a range of heights versus one 24-h day by averaging over a given number of days. The 24-h time axis was chosen in order to demonstrate the existence of tidal periodicities present in the data. The intensity (power) of the reflected signal is color-(shade-) coded of the averaged power converted to dB.

Fig. 1 introduces the ionosonde HTI displays which were computed from sequential ionograms. These were recorded with a CADI which operated on the Aegean island of Milos during the summer of 1996. Fig. 1 includes four 24-h HTI plots averaged over a period of 6 days, from July 31, 1996 to August 05, 1996. The four plots correspond to different radio frequency ranges, namely, 1.5–3.0 MHz (upper left), 3.0–4.0 MHz (upper right), 4.0–5.0 MHz (lower left), and 5.0–7.0 MHz (lower right). As expected, the displays differ because each depicts ionospheric changes in electron density at different reflection heights which depend on the sounding frequencies. As seen from the low-frequency (1.5–3.0 MHz) HTI plot, the upper ionosphere is masked during sunlit hours, from about 06–18 h local time (LT), because of the build up and zenith angle control of the E region, whereas the rise and fall of the F region bottom-side is well marked during nighttime. On the other hand, the higher frequency HTI plots, e.g., see the bottom panels in Fig. 1, show considerable temporal structure at upper heights during the entire day, most likely caused by dynamic processes in the F region.

The most consistent signature in the HTI plots of Fig. 1 are the striations seen below about 130 km. These are attributed to the sporadic E layers. A pronounced semidiurnal periodicity is observed, marked by the two consecutive traces of reflected power, one occurring during daytime from about 06 to 18 h LT followed by a nighttime trace from about 18 to 05 h LT. Both traces start at about 125 km and then move steadily downward. This downward sloping of the E_s traces portrays the well-known descending character of sporadic E. Further inspection shows that the nighttime E_s trace is stronger than the daytime one, causing also images to appear in altitude due to multiple E_s-ground reflections. This is at least partly and maybe completely due to reduced ionospheric absrorption at night. Another point implied from the HTI plots in Fig. 1 is the transparency of E_s, so that upper heights become also detectable, a fact which is compatible with the patchy character of sporadic E (Whitehead, 1989).

Inspection of numerous HTI plots of the type shown in Fig. 1 suggested that the HTI display is particularly useful for studying sporadic E layer dynamics and variability. An advantage dealing with sporadic E is that there is very little

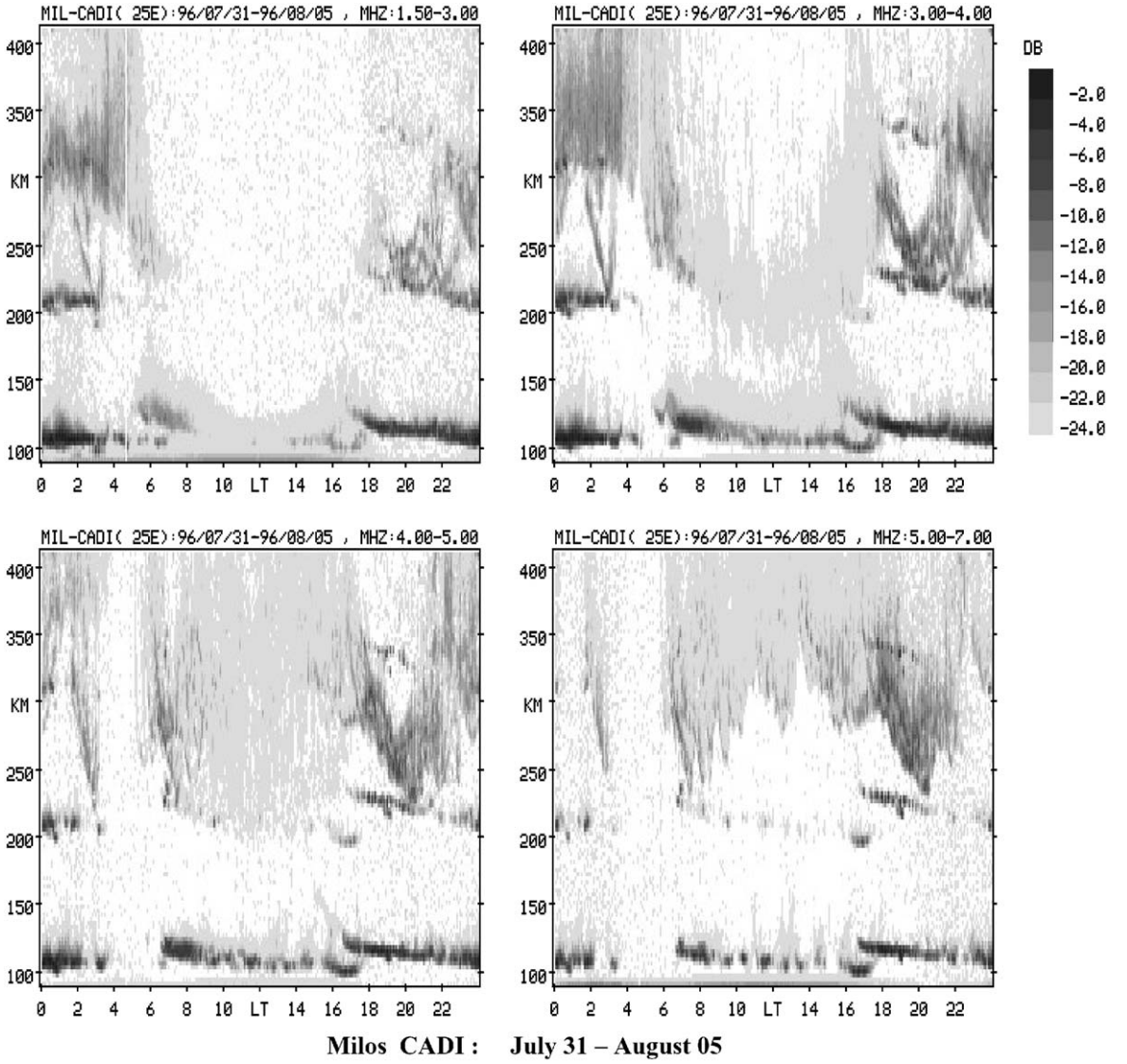

Fig. 1. Typical examples of CADI ionogram HTI plots computed for a 24 h day, averaged over six consecutive days. Each plot corresponds to a different ionosonde frequency band, marked at the top right corner in each figure. The slopping striations between 100 and 130 km are sporadic *E* layer traces.

magnetoionic splitting because these are thin layers confined in altitude in the lower ionosphere. Note also that for frequencies significantly higher than *foE* there is little, if any, group retardation of the incident radio wave, that is, the echo delays give real heights.

3. Experimental results

The Milos CADI (geographic location 36.7°N, 24.5°E, magnetic latitude 30.8°, magnetic dip 52.5°, magnetic declination 2.5°) operated continuously from June 23, 1996 to September 30, 1996. It was programmed to perform a 54-s frequency sweep, consisting of 250 steps from 1.5 to 16.0 MHz, every 5 min during daytime and every 2 min during nighttime from 1900 to 0500 hours universal time (UT) (LT = UT + 1.7 h). The Milos site was nearly free of man-made interference, and the measured ionograms were of good quality. Inspection of the observations showed the presence of a fairly continuous and often intense E_s activity from late June to early September, which makes the present data representative of midlatitude E_s at summertime.

The ionogram HTI analysis was applied for a 24-h daytime base starting at 06 h LT. Because of the variable nature of E_s, HTI plots averaged over several sequential days were found to be statistically more appropriate in defining long-term trends in the data. This was shown in Fig. 1, which illustrates a prevailing semidiurnal pattern in occurrence and altitude descent of sporadic E from July 31 to August 5. To appreciate the variability and intermittency of E_s on a day to day basis, we provide in Fig. 2 single day HTI plots from July 31 to August 5, which are used to produce the average shown in Fig. 1.

The HTI displays in Fig. 2 were computed at the fixed frequency band between 3 and 4 MHz, for altitudes between 90 and 250 km. As seen, the semidiurnal character of layer formation and height descent prevails in nearly all days. Seen are two main striations of E_s reflected power, the daytime one staring at about 120–125 km near sunrise (06 h LT) and the nighttime one starting at about the same altitude near sunset (18 h LT). Both traces are negatively tilted with time due to the downward transport of the layers. The reflected signal can disappear and reappear but, it is interesting to note, that this "on–off" sequence occurs mostly along the layer's descent trace, which is defined better in the averaged HTI plots of Fig. 1. Also in most of the plots in Fig. 2, the start of the E_s striations connect to upper E region through weak reflection traces which also descend with time but at much higher rates, estimated to be in the range of 5–8 km/h. These identify with the well-known intermediate layers which, according to several Arecibo ISR studies (e.g., see review of Mathews, 1998), have a strong semidiurnal character, forming two times a day at the bottom of the F region and moving downward.

Although at times the intermediate layers can also be traced in the HTI plots, in most instances they are not, because they are weak, having low critical frequencies below the lowest ionosonde frequency of 1.5 MHz. Also one has to be aware that at these low-ionosonde frequencies propagation effects are more significant. Therefore, the estimated heights can be affected more by group retardation and thus can be incorrect relative to the real heights. Despite these limitations however, the present HTI plots can provide some information on the descending intermediate layers as well, which agrees also with previous ionosonde studies, e.g., see Wilkinson et al. (1992).

3.1. Descending sporadic E layer patterns

The situation shown in Fig. 3 is typical and resembles that in Fig. 1. It shows four HTI plots, averaged over 5 days (from August 25 to 30) inside four different frequency bands: 1.5–2.5 MHz (upper left), 2.5–3.5 MHz (upper right), 3.5–4.5 MHz (bottom left), and 4.5–5.5 MHz (bottom right). As seen, there exist two downward-sloping E_s striations well separated during the 24 h course, marking descending sporadic E layers which occur with a striking semidiurnal periodicity. The layers form at about 120 km, one near sunrise (~06 h LT) and the other about 12 h later at about ~18 h LT. Both layers move downward with time to heights less than 100 km where they gradually become unobservable. The daytime layer descends at rates $dz/dt \sim 1.4$ km/h relative to the nighttime layer descent speed of ~1.8 km/h, and it lasts longer. For example, in the 1.5–2.5 MHz HTI plot the morning layers are traced from 06 to 22 h LT.

The HTI plots in Fig. 3 show the E_s traces to start earlier and end later at lower rather than higher ionosonde frequencies. This means that, as the layer moves down from its 120–125 km level first its electron density N_e rises, apparently because of the ongoing metallic ion accumulation, thus reaching a peak at a lower height (say near 110 km) where production equals loss. Then, as the descent continues to lower altitudes N_e appears to decrease gradually until the layer passes undetected because its critical frequency becomes smaller than the lowest ionosonde frequency. The layer depletion at lower heights is attributable to the much shorter lifetimes of metallic ions at these altitudes (e.g., see MacDougall et al., 2000). Although the HTI plots here detect the layers down to about 100 km, the layer descent should continue to lower heights. This is clear from the sensitive ISR observations at Arecibo which show descending layers to become steadily weaker and reach $N_e \sim 300-500\,\mathrm{cm}^{-3}$ down to 95–90 km level (Mathews, 1998).

Finally, the HTI plots shown in Fig. 4 are representative of times near the summer solstice when mid-latitude E_s is known to be the strongest. Again, Fig. 4 includes four HTI plots, averaged over 6 days from June 30 to July 5 and corresponding to four different frequency bands, that is, 1.5–3.0, 3.0–4.0, 4.0–5.0, and 5.0–6.0 MHz from top left to bottom right. Compared to Fig. 3, two downward-inclined E_s traces can again be observed, which now are more closely spaced in height and may overlap

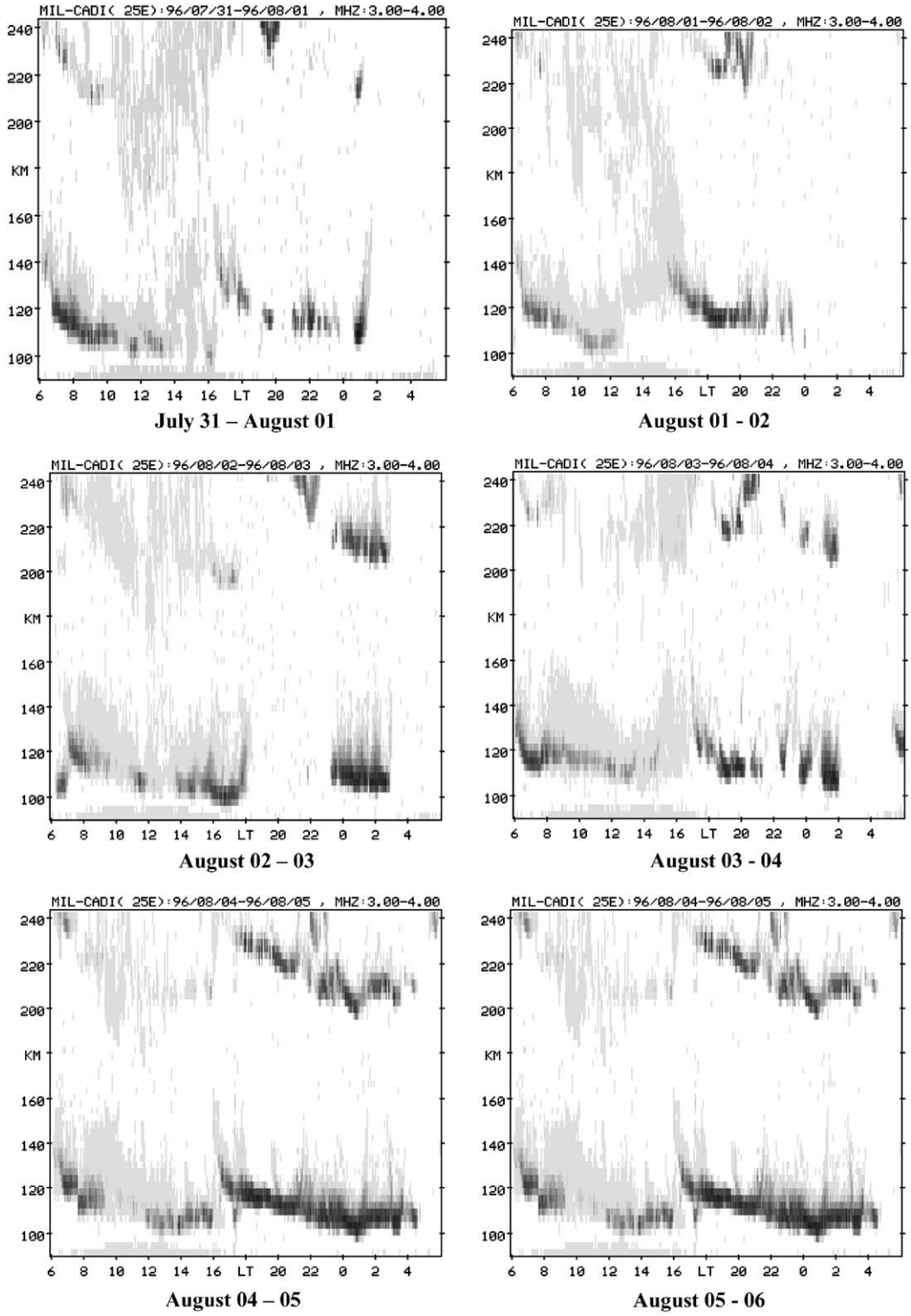

Fig. 2. HTI plots for each of the 6 days used to compute the averaged HTI displays shown in Fig. 1. All plots are computed for the ionosonde frequency band between 3 and 4 MHz, and for altitudes between 100 and 250 km. The 24 h time axis is in LT starting at 06 h. Despite the variability and intermittency from day to day, there is a regular pattern seen in sporadic E layer occurrence and altitude descent which is dominated by a semidiurnal periodicity. Also seen is a close relation to the upper E region descending intermediate layers.

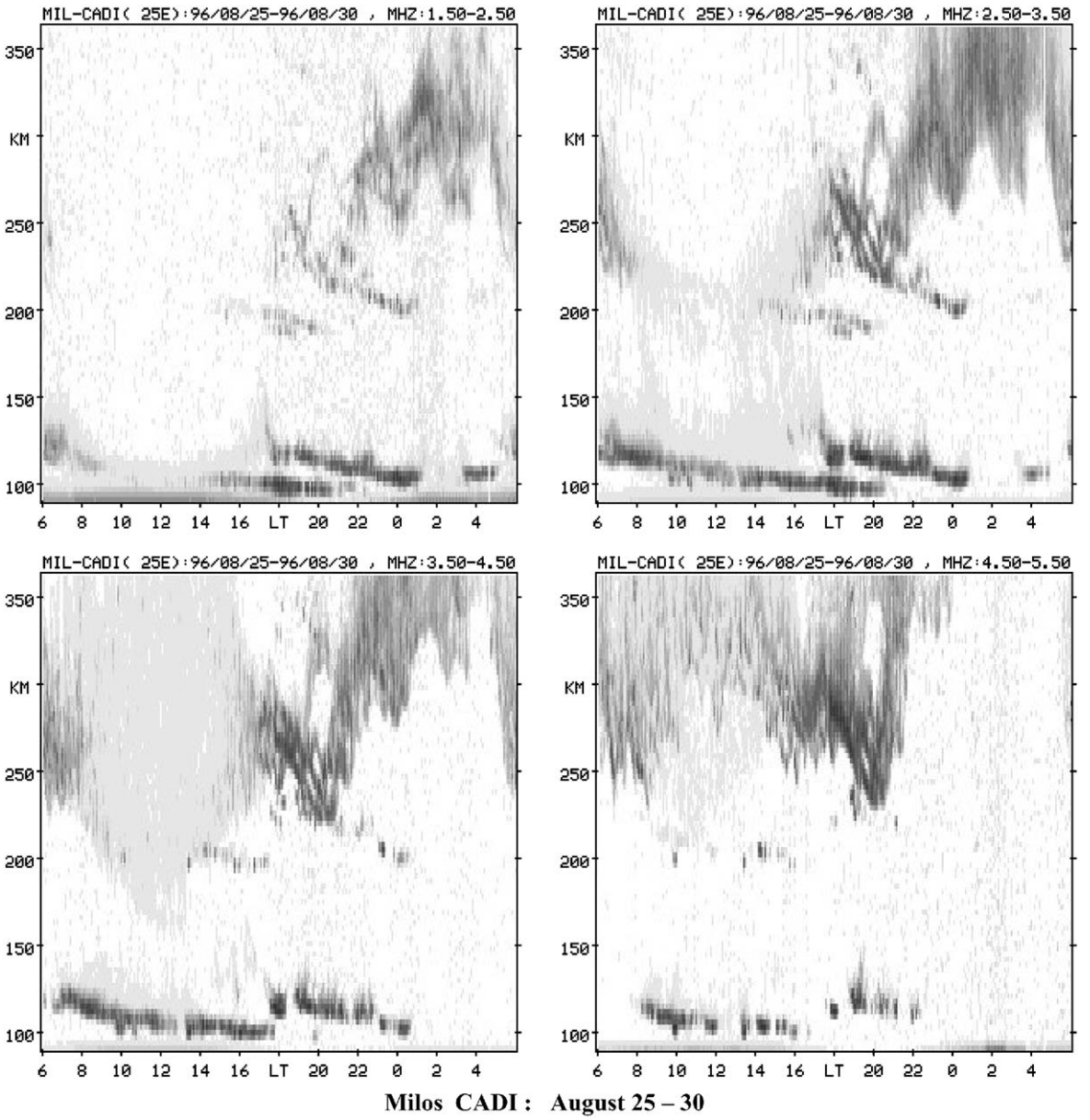

Fig. 3. Milos CADI HTI plots averaged over 6 days from August 25–30, 1996. The descending sporadic *E* layers appear with a striking semidiurnal periodicity. As seen, a daytime layer starts near 120 km at about 06 h LT, followed by a nighttime layer 12 h later. Both layers move downward with descent rates near 1.4 and 1.8 km/h, respectively.

in time for many hours during the day. The first trace starts near 125 km at about 05 h LT, whereas the second becomes detectable near 130 km at about 10–11 h LT. Both these HTI striations are tilted downward with time, having slopes ranging between 0.8 and 1.1 km/h. Contrary to the cases presented in Figs. 1 and 3, the situation in Fig. 4 indicates a much weaker semidiurnal effect.

3.2. Sporadic E layer descending trends during summer

As mentioned, the CADI observations covered the interval from June 23 to September 20, 1996. Detailed HTI analysis suggested some systematic differences in the descent of sporadic *E* layers as time progresses from solstice to equinox. In this

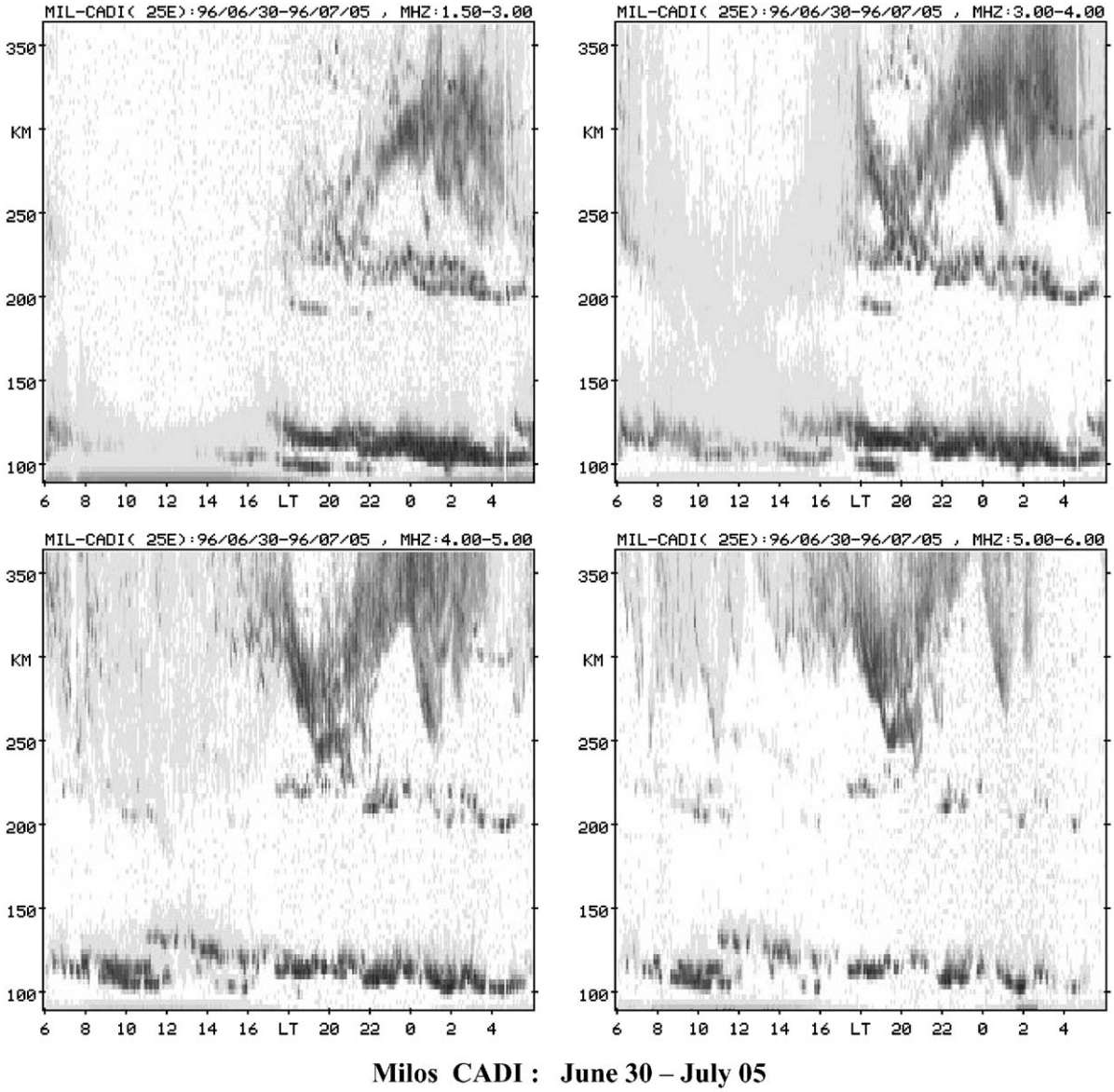

Fig. 4. Same as Fig. 3 but for a time interval near the summer solstice. See text for more details.

section we summarize the average trends in layer descent which may be of significance for the diurnal and seasonal sporadic E variability. We recognize, however, that the general validity of these results cannot be established from a single summer analysis and that ionogram data from more summers need to be studied.

Fig. 5 shows three HTI plots covering the observations from June 23 to the end of July, 1996. All plots were computed for ionosonde frequencies between 4.0 and 7.0 MHz which are higher than the anticipated E region critical frequencies foE. Thus, the measured (virtual) E_s heights are near to the real ones.

The upper and middle panel in Fig. 5, which correspond to the last week of June and the first 3 weeks of July, respectively, show a dominant diurnal periodicity in E_s layer descent. A layer first appears at about 115 km near 05 h LT and then is seen to move slowly down toward 100 km for more than 12 h until it becomes undetectable. This trace, which is attributed to a convergence node of the diurnal tide, is followed by a second one that appears during the day at about 120 km undergoing

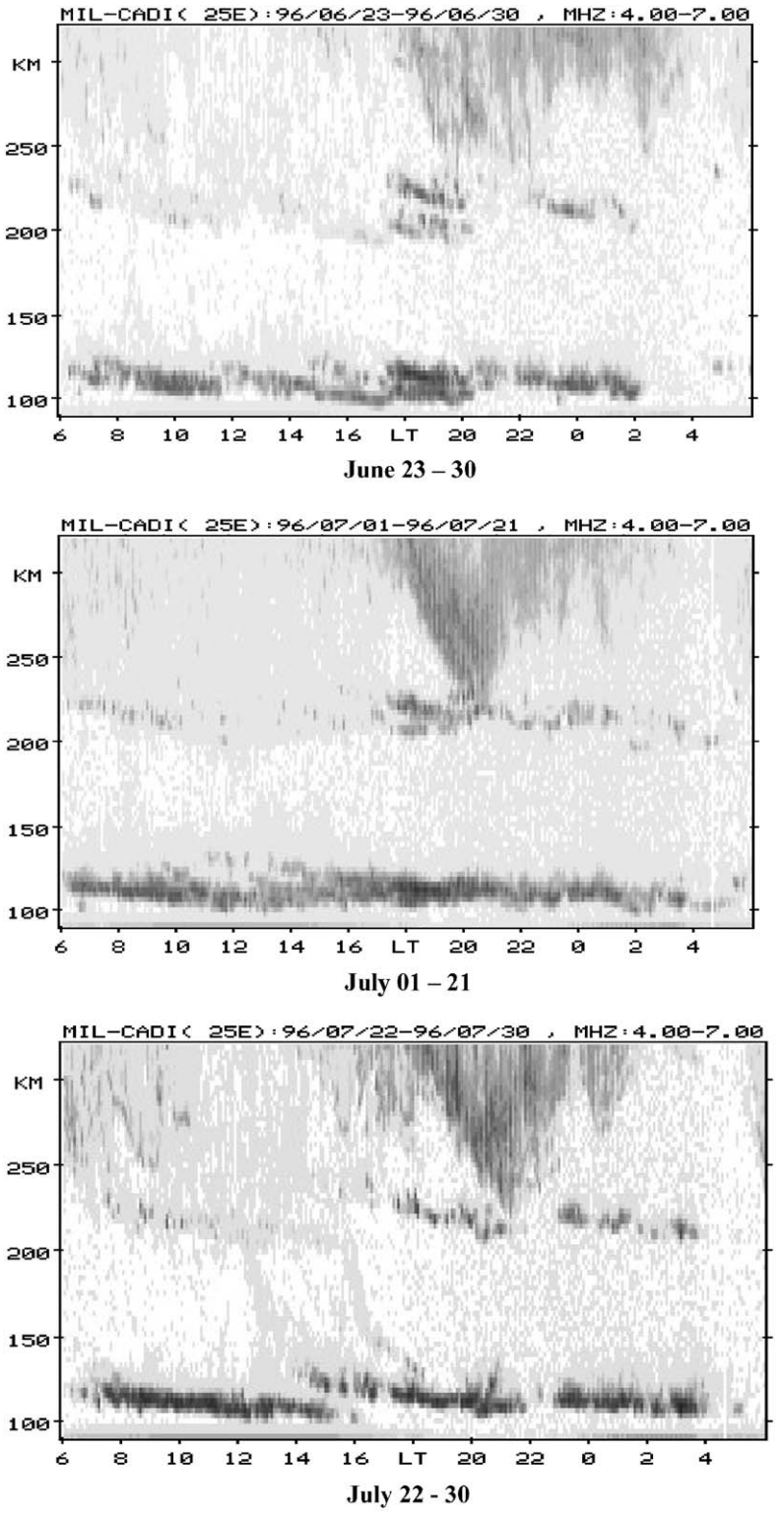

Fig. 5. Averaged HTI plots representing sporadic *E* layer descent and variability for times near summer solstice (from June 23 to July 31).

a slow downward motion through the entire night and into the morning sector. This is considered again to be due to a subsequent convergence node of the diurnal tide. Note that the vertical (altitude) separation of the two layers is close to about 20 km, and represents here the vertical wavelength of the diurnal tide.

A weak semidiurnal effect is seen clearly in the upper panel of Fig. 5 (during June 23–30) but this is obscured in the middle panel, although it is also present there as well at least for part of the time interval under consideration (e.g., see also the HTI plots in Fig. 3 which correspond to the interval from June 30 to July 5). Finally, the HTI plot at the bottom of Fig. 5 corresponds to the last week of July. It shows the HTI plot to be dominated by three sloping E_s traces, distributed more or less evenly during the 24-h day, which are attributed to the effects of a terdiurnal tide. The presence of a strong terdiurnal periodicity in the same Milos data during the last days of July has been first recognized and reported in a separate study by Haldoupis et al. (2004).

Estimates of descent rates in the interval from June 23 to July 31 take values between 0.8 and 1.3 km/h, with an average near 1.0 km/h. If we assume that on average the layers descend with the phase velocity of the diurnal tide, then this corresponds to a vertical wavelength of about 25 km, which is close to the theoretical wavelength of 28 km of the $S_{1,1}$ diurnal tidal mode (Forbes, 1984).

Fig. 6 shows the situation prevailing for the rest of the Milos CADI data, from August 1 to September 20, when sporadic E is known to become gradually weaker with time, past the summer solstice (Whitehead, 1989). The upper and middle panel in Fig. 6 are HTI averages for the periods from August 1 to 15 and from August 16 to 31, respectively, whereas the bottom panel refers to the entire month of September. As seen, there is a semidiurnal periodicity present in all HTI plots which is more pronounced in the lower two panels. On average, we observe two well separated and negatively sloping traces which correspond to a daytime and a nighttime sporadic E that form around 120 km at about 06 and 17 h LT, respectively, and descend to lower heights with time, as discussed also in Figs. 1 and 3. The descent rates were found to be 1.4 ± 0.2 and 1.9 ± 0.3 km/h, for the daytime and nighttime layers, respectively. These values are consistently larger than the descent rates measured earlier in the summer during the first weeks of July.

3.3. Periodicities in foEs

The HTI plots show a weak semidiurnal pattern in E_s layer descent during June–July which becomes stronger in the late summer during August–September. This is also supported from the analysis of the corresponding E_s critical frequency, *foEs*, time series. Note that *foEs* is expressed in MHz and used widely to quantify the sporadic E layer variability. In a recent paper by Haldoupis et al. (2004), the Milos CADI *foEs* data were used to study the tidal and planetary wave periodicities in sporadic E electron densities. It was shown that, besides the leading roles of the diurnal and semidiurnal tides in E_s formation and strength, there is often also a weaker but significant contribution from the terdiurnal tide. This is confirmed also here by the HTI analysis, as seen for example at the bottom plot of Fig. 5. Note that, Haldoupis et al. (2004) have shown that both the semidiurnal and terdiurnal spectral peaks are real 12 and 8 h periodicities and not harmonics of a distorted diurnal oscillation.

Fig. 7 summarizes the Milos *foEs* measurements from June 27 to July 21, when the diurnal tidal control of E_s layer descent is clearly present in the HTI plots. The *foEs* time sequence is made of 10-min samples and is plotted in the top panel whereas its amplitude spectrum is plotted below. As seen, both the *foEs* time series and spectrum are dominated by a strong peak at 24-h, whereas much weaker peaks in the spectrum exist at 12 and 8 h, suggesting also a role for the semidiurnal and terdiurnal tides. Finally the bottom plot in Fig. 7 shows the mean diurnal variation of *foEs* averaged over the June–July time interval under consideration. This is dominated by a main peak which suggests a dominant diurnal periodicity. This peak occurs prior to local noon near 10 h LT, a fact that has been well known for many years, although it is still not well understood (Whitehead, 1989). A weaker peak is also seen near 18 h LT, about 8 h apart from the strong peak near 10 h LT, caused most likely by the action of the terdiurnal tide which was also present in the data. Note that in the last plot there is no clear evidence for a semidiurnal periodicity.

Finally, Fig. 8 is the same as Fig. 7, but it refers to the August 01–31 period when there is a clear

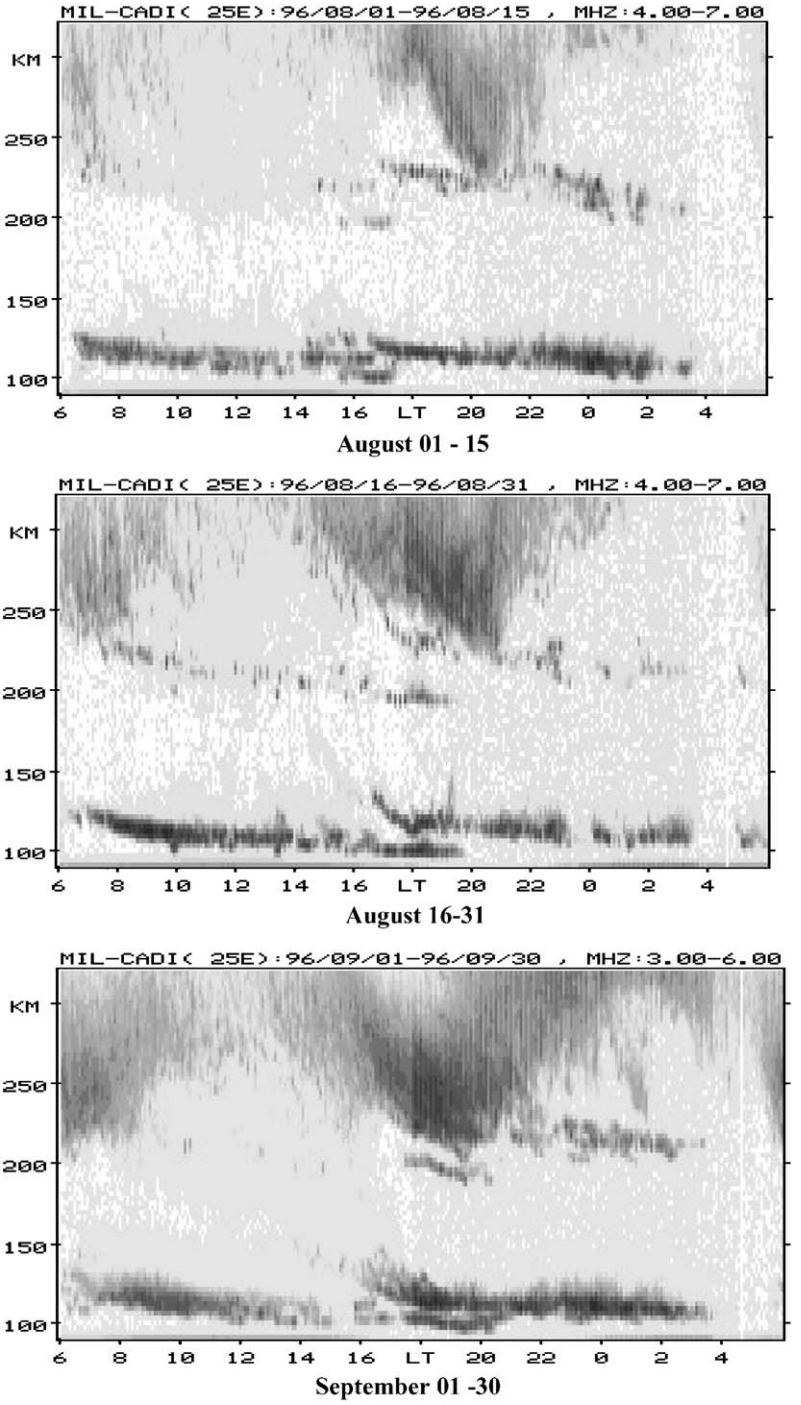

Fig. 6. Same as in Fig. 5, but for later in the summer, from August 1 to September 21. During these times the observed semidiurnal periodicity intensifies and dominates the layer descent and diurnal variability.

semidiurnal control on the layer formation and descent. This 12-h periodicity revealed by the HTI plots is also embedded in *foEs* as well, as shown in the corresponding amplitude spectrum plotted in the middle panel of Fig. 8. As seen, there is a 12-h peak that is equally strong as the 24-h (diurnal) periodicity, in contrast with the situation in Fig. 7. Furthermore, the mean diurnal variation during

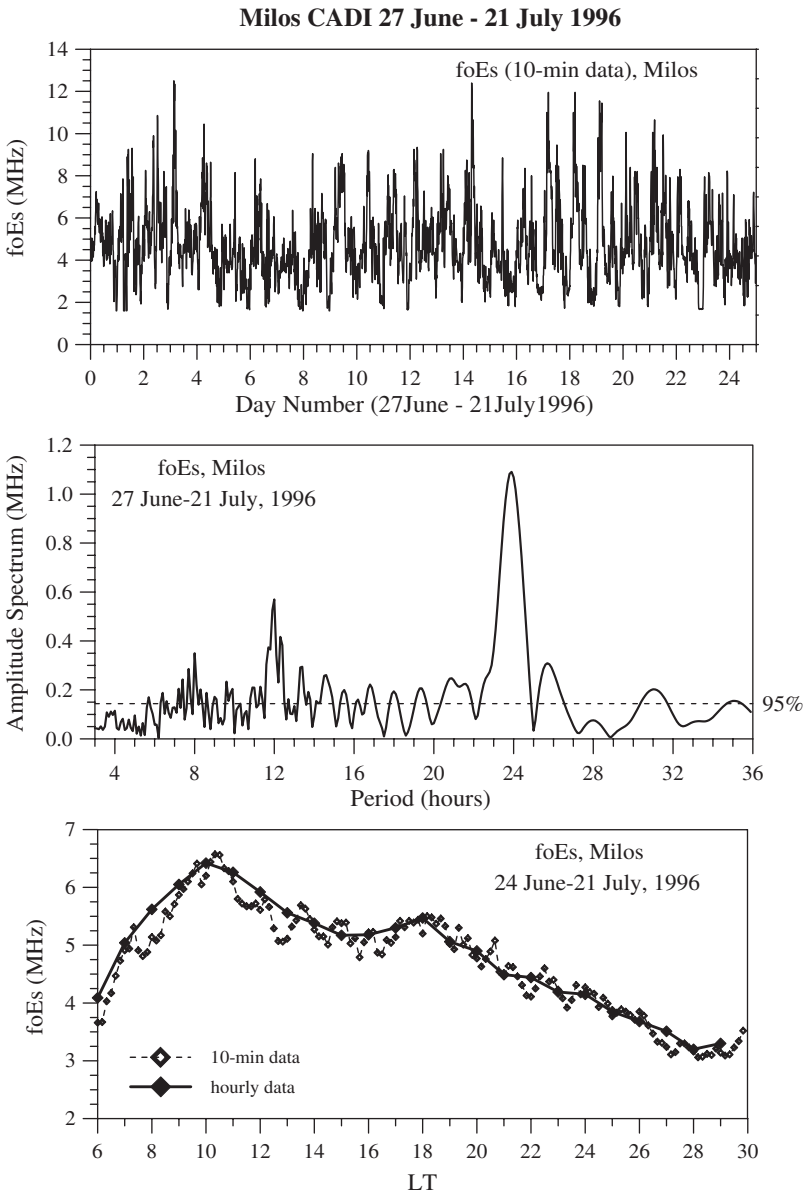

Fig. 7. Critical sporadic *E* frequency (*foEs*) analysis for the period from June 27 to July 21, near summer solstice. The upper panel is the hourly means time series, the middle panel is the corresponding amplitude spectrum, and the bottom plot shows the mean daily variation starting at 06 h LT. The diurnal periodicity dominates.

August, which is presented in the bottom panel, shows a well-defined secondary peak in *foEs* around 22 h LT, about 12 h away from the strongest peak near 10 h LT. It is interesting to note that similar results (not shown here) were also obtained by analyzing Rome ionosonde data for the same time intervals of 27 June–21 July and 01–31 August, 1996.

4. Comparison with ISR observations

As summarized in the review paper by Mathews (1998), the regular occurrence as well as the vertical motion and variability of mid-latitude sporadic *E* are shaped by the semidiurnal and diurnal tides in the lower thermosphere. The tides can provide downward propagating wind shears of ion

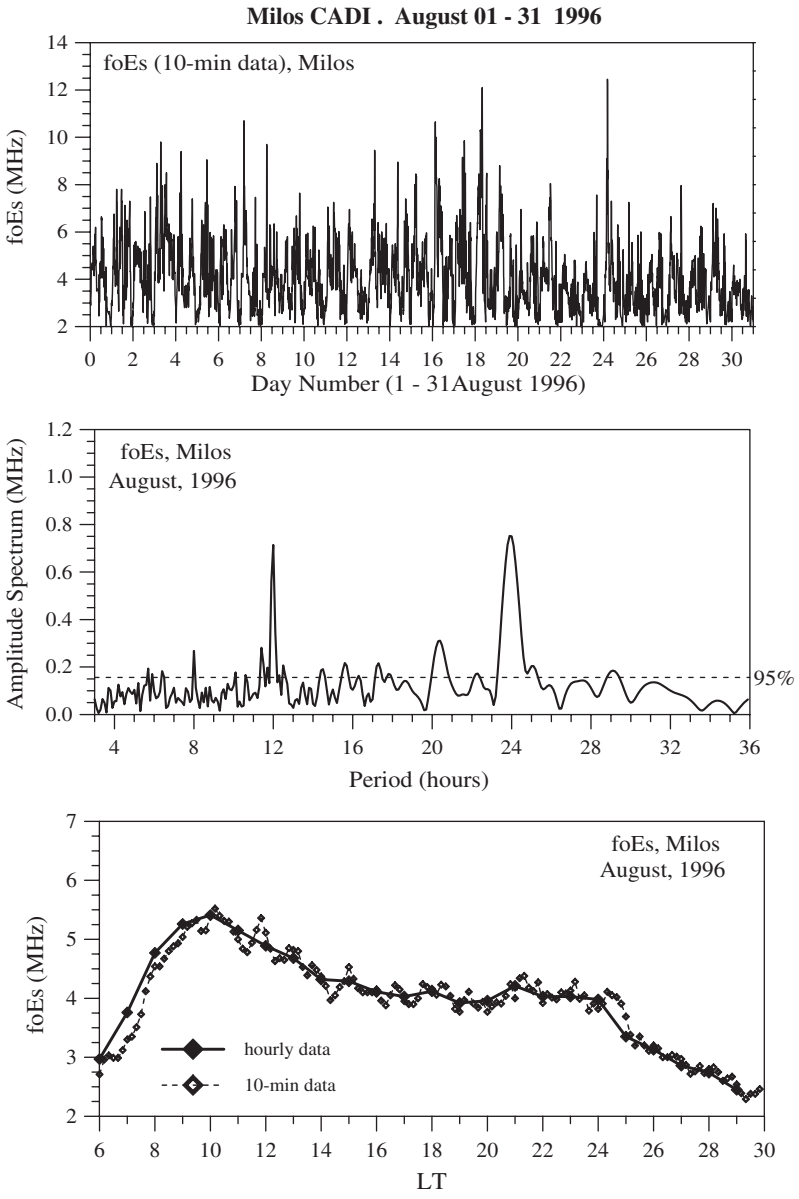

Fig. 8. Same as Fig. 7, but for the month of August, showing the presence of a strong semidiurnal periodicity in *foEs*, in line also with the HTI plots in Fig. 6.

convergent nodes, which can account for the formation and vertical transport of the layers, as was shown theoretically by Axford (1963), numerically by Chimonas and Axford (1968), and experimentally by Mathews and Bekeny (1979) using Arecibo ISR observations.

The Arecibo ISR studies revealed a regular semidiurnal pattern for the descending intermediate layers in the upper *E* region, a dominant diurnal periodicity for the lower *E* region sporadic layers, and a confluence zone between about 120 and 100 km where both tidal modes can be active. Tong et al. (1988) presented continuous layer motions obtained from Arecibo height–time layer trajectories observed during January 3–6, 1981 and November 8–10, 1985. Inspection of these plots show: (1) A once-per-day periodicity for the daytime sporadic *E* layers forming near 115 km at about 0600 h LT and descending down to 90 km with a speed of about 1.1 km/h. (2) A twice-per-day

periodicity for the intermediate layers at upper heights that move fast down to 120 km with speeds ranging between 5 and 8 km/h, while at times the situation can be complicated by the additional action of a quarterdiurnal tide in the upper E region. (3) Although not emphasized in the Tong et al. (1988) paper, the plots show also an once-per-day weaker E_s trajectory caused by nighttime sporadic E layers forming near 120 km at about 1600–1800 h LT and moving downward with speeds near 2.0 km/h.

In comparing the ionosonde and ISR observations, one should bear in mind that the ionosonde is much less sensitive because it needs electron densities N_e larger than $\sim 5 \times 10^4\,\mathrm{cm}^{-3}$ in order for its signal to be totally reflected. This means that ionosonde E_s layer returns are biased to altitudes between about 100 and 120 km where the layers are strongest. As for the intermediate layers above 130 km usually these go unnoticed by the ionosonde because they are not dense enough to cause total reflections and/or because of blanketing effects from the strong layers below. On the other hand, the Arecibo results are based on a few limited observational periods mostly during winter, whereas the CADI HTI results cover the entire period from the summer solstice to equinox.

Despite the sensitivity limitations, the present ionosonde results are in reasonable agreement with several of the ISR characteristics of sporadic E layer descent and occurrence. Namely, the HTI plots show the presence of daytime and nighttime E_s layers that form near 120 km around 0600 and 1800 h LT, respectively, which then descend steadily with height at rates dz/dt that are comparable with ISR estimates. Also, the faint HTI traces seen at times well above 130 km occur mostly with a semidiurnal periodicity and have descent rates dz/dt between 5 and 8 km/h, which again compare well with the Arecibo observations of intermediate layers. On the other hand, there are also differences between the ionosonde and ISR findings. For example, the ionogram HTI plots show, in line with previous ionosonde studies (e.g., see MacDougall, 1974; Wilkinson et al., 1992; Szuszczewicz et al., 1995), that the twice-per-day periodicity in E_s layer descent and occurrence is much more pronounced than the prevailing diurnal periodicity seen in the Arecibo E_s observations (Mathews, 1998). Moreover, the current data suggest a terdiurnal periodicity being often present during summer, a fact that has not been identified so far with the Arecibo ISR. These discrepancies however might be expected because long-term Arecibo observations of sporadic E are limited and the existing ones may not be representative of the average summer conditions dealt with in this ionosonde study.

5. The physical picture

As Mathews (1998) points out in his review paper, the prevailing periodicities in mid-latitude sporadic E result from the confluence of the vertical tidal wind shears in the lower thermosphere, particularly in the altitude range between 100 and 120 km. The observed diurnal, semidiurnal and terdiurnal periodicities, seen in the occurrence, altitude descent and strength (*foEs*) of sporadic E, show the decisive role played by the atmospheric tides which provide the convergent wind shears needed for the layers to form and build up, while tidal phase progression downward causes their altitude descent. Next, we rely on present and past evidence to interpret our main results as follows.

We start with the pronounced semidiurnal periodicity in E_s, manifested in the ionosonde HTI plots by a daytime and a nighttime descending layer. This can be attributed to the semidiurnal character of the DIL which act as suppliers of metallic ions for the lower E region. DIL form in the upper E region inside a convergent node in the vertical wind profile associated with a downward propagating semidiurnal tide. According to wind shear theory, a layer remains at the shear convergence null only if it forms fast compared with the time required for the null to propagate downward a distance equal to the layer's width (e.g., see Chimonas and Axford, 1968). In the upper E region, the layers form rapidly because the ion–neutral collision frequency is small, therefore they tend to "stick" at the wind shear convergence null as this moves down with the tidal vertical phase velocity.

At heights below about 125–120 km the situation changes because ion–neutral collisions become increasingly effective. There, the downward transport of intermediate layers slows down because vertical ion convergence becomes slower, thus the layers cannot form fast enough in order to remain inside the tidal convergence null as in the upper E region. In effect, the layers lag steadily behind the tidal convergence null, thus descending at rates increasingly smaller than the vertical phase velocity of the tide. This slow descent continues until the following divergent node catches up with the layer,

to impose small layer uplifts and some vertical plasma divergence that may disrupt and disperse the layer. Finally, and depending upon the amplitude and phase velocity of the semidiurnal tide, there is a lower altitude at which the ion–neutral collision frequency is high enough, so that it does not allow the 12-h tide to have any effect on the layer.

In line also with the Arecibo ISR observations (e.g., see Tong et al., 1988), the morning E_s layer, which starts at about 120 km near 06 h LT and moves steadily down to 100 km by the evening, is attributed mainly, but not fully, to the diurnal $S_{1,1}$ tide which is known to dominate in the lower E region, e.g., see Harper (1977). On the other hand, the semidiurnal tide must also contribute in the morning E_s formation as well. This is supported by the fact that often the morning sporadic E layer is born out of a DIL reaching 125 km at about 06 h LT. By assuming the 12 and 24-h tidal convergence nodes to be approximately in phase, their action combines in the morning hours to reinforce E_s. This process may lead to the well-known pre-noon maximum in E_s layer occurrence and strength near 110 km at about 1000 h LT, as manifested by the layer's critical frequency E_s daily peak (Whitehead, 1989).

As time progresses, the semidiurnal tidal effect on the daytime layer ceases because the 12-h convergence null moves fast downward at phase speeds between 5 and 8 km/h so it leaves the layer behind. On the other hand, the daytime layer can respond to the 24-h tidal forcing and can be transported down with the vertical phase velocity of the diurnal tide which is considerably smaller than that of the semidiurnal tide. The observed mean descent speeds for the morning layers range from 0.8 to 1.6 km/h, which compare well with the vertical phase velocities of the diurnal tides having wavelengths between 20 and 40 km, respectively.

The nighttime sporadic E layer which appears at about 1800 UT near 125 km, is weaker, has shorter duration, and descends faster relative to the daytime layer. Since it cannot be associated with the diurnal tide, it is interpreted as being due to the intrusion and intensification of the daytime DIL into the lower E region under the action of a vertical wind shear associated with the semidiurnal tidal wind profile. The observed descent rates between 1.7 and 2.2 km/h for the nighttime E_s can be explained as the result of increased collisions which slow the layer descent relative to the phase velocity of the tide. The faster descent rates for the evening layer and its reduced layer strength and duration relative to the daytime layer, are properties which favor the semidiurnal tide as the main driver during nighttime hours.

The diminished semidiurnal periodicity seen during several days of observations, especially during periods near solstice, can be understood as the result of weakening of the semidiurnal tidal activity in the upper E region. In the same way, the terdiurnal periodicities seen occasionally can be interpreted as being due to enhanced terdiurnal tidal action in the upper E region and their mixture with the diurnal and semidiurnal tides inside the sporadic E confluence zone between 100 and 130 km.

6. Numerical simulation

In order to substantiate the interpretation above, we performed a numerical simulation of intermediate and sporadic E layer vertical trajectories by using the methodology introduced first by Chimonas and Axford (1968). In modeling the layer vertical motions, we solve numerically Eq. (1), which is a first-order ordinary differential equation, $dz/dt = w(z, t)$, by using a varying time-step fourth-order Runge–Kutta algorithm with a maximum allowed time-step of 10 s. In solving Eq. (1) we use an oversimplified wind system that is dominated by a semidiurnal tide in the upper E region and a diurnal tide at lower E region, in line with existing Arecibo observations (e.g., see Harper 1977) and the E_s modeling methodology of Mathews and Bekeny (1979). For clarity, the numerical results were obtained by using only a zonal horizontal wind component, thus meridional wind U was set to zero in Eq. (1), while the zonal wind profile V was set equal to

$$V = V_0 \exp\left(\frac{z - z_0}{2H}\right) \cos\left[\frac{2\pi}{\lambda_z}(z - z_0) + \frac{2\pi}{T}(t - t_0)\right], \tag{2}$$

for both the 24- and 12-h tidal winds which were added to get the total wind system.

In the last equation, T and λ_z are the period and vertical wavelength of the tidal wind, H is a representative scale height for the lower thermosphere between 80 and 200 km, z_0 is a lower altitude boundary set equal to either 85 km for diurnal, or 95 km for semidiurnal tides, and t_0 is the phase of the tide at the representative scale height. The ion–neutral collision frequency profile between 80

and 200 km was based on a least-squares fit of the ν_i/ω_i altitude data used by Bishop and Earle (2003) as being more appropriate for metallic ion plasma in the lower mesosphere. With respect to the tidal parameters, these were kept similar to the ones used by Tong et al. (1988) for the diurnal (semidiurnal) tide: $T = 24\,\text{h}$ (12 h), $\lambda_z = 25\,\text{km}$ (90 km), $V_0 = 20\,\text{m/s}$ (3 m/s), $z_0 = 85\,\text{km}$ (95 km), $t_0 = 9\,\text{h}$ (5 h), $H = 5.5\,\text{km}$ (5.5 km). Based on the tidal wavelengths, the downward phase velocities for the diurnal and semidiurnal tide were near 1.1 and 7.5 km/h, respectively.

Typical numerical results for the tidal ion layer trajectories are grouped in Fig. 9. The solid and dashed lines correspond to altitude versus time trajectories of metallic ion layers that form within a convergent node of a vertical wind shear in the diurnal and semidiurnal sinusoidal wind profiles, respectively. The shear convergent nodes were launched at about 120 km for the diurnal and 200 km for the semidiurnal tide, and this pattern was repeated every 24 and 12 h, respectively. The time axis in Fig. 9 starts at 06 h LT, in order for these results to compare with the ionosonde HTI observations presented earlier.

As expected by the wind shear theory, the net downward layer transport follows the phase velocity of the tidal convergent node at higher altitudes where slopes are straight lines. This applies down to a level where the enhanced ion–neutral collisions act to slow down the layer's descent until this reaches a stagnation altitude or "dumping level", a term first introduced by Chimonas and Axford (1968). There, and only in principle, the layer can oscillate slightly in height with the tidal period under the forcing of consecutive convergent and divergent wind shear nodes as they move downward across the layer's dumping level. Given that the shear horizontal wind polarity is fixed, the model shows that the layer stagnation level depends primarily on the vertical tidal wavelength, or its phase velocity, and secondarily on the tidal wind amplitude.

For the adopted tidal parameters given earlier, Fig. 9 shows that the 1.04 km/h downward phase speed of the 24-h tide is slow enough to bring an ion layer along a convergent node down to about 95 km where it starts slowing down and reaches stagnation at about 85 km. For the upper E region semidiurnal tide, which has a vertical wavelength of 90 km (near to that of a $S_{2,3}$ tide) and thus a downward-phase velocity of 7.5 km/h, the downward-moving layer trajectory starts departing from a straight line at about 135 km in order to reach gradually its stagnation level at about 105 km.

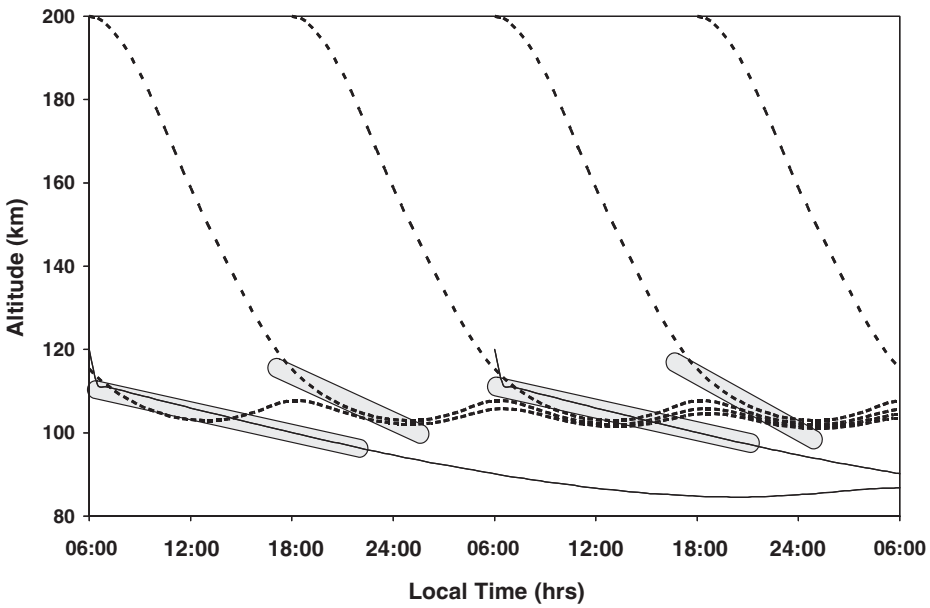

Fig. 9. Numerical simulation results based on basic wind shear theory predictions and a oversimplified tidal wind system dominated by a $S_{2,3}$ semidiurnal tide in the upper E region and a $S_{1,1}$ diurnal tide in the lower E region. The curves shown (solid and dashed) correspond to metallic ion layer trajectories that form inside convergent nodes of vertical wind shears in the tidal wind which move downward with the vertical phase velocities of the tides. The inclined bars represent the anticipated traces of sporadic E, and they are sketched in for clarity purposes. See text for more details.

The shaded, downward tilted, bars in the lower part of Fig. 9, which are sketched in to be parallel to the predicted ion trajectories, depict the alternating daytime and nighttime sporadic E layer traces which are expected to form between 100 and 120 km. As seen, for the descending daytime sporadic E layer there is an interval of several hours, from about 06 to 14 h LT, where there exists a confluence of the 24- and 12-h tides between about 120 and 105 km. There, the descending intermediate layer, which is brought down from the upper E region by the semidiurnal tide (dashed lines), is transferred fully into the slowly descending convergent node of the diurnal tide (solid lines). It is interesting to note that this is the time interval when the strongest E layers are observed, with critical frequencies *foEs* reaching their daily peak near 10 h LT.

As for the evening and night hours, when the nighttime E_s layer forms, Fig. 9 shows no confluence between the 12- and 24-h tidal convergent nodes because they are well separated in height, thus the E_s layer forming process is controlled only by the semidiurnal tide. This tide transports the daytime DIL down into the lower E region where its descent is slowed down considerably by collisions relative to the phase velocity of the tidal convergent node. According to Fig. 9, the daytime intermediate layer can form the core of the nighttime sporadic E which, as the observations show, is weaker, it has shorter duration, and reaches bottom heights not as low as the morning (or daytime) layer. These model inferences are in good agreement with the ISR observations of nighttime sporadic E shown in Tong et al. (1988).

It is also interesting to note that the shaded bars along the layer trajectories, which act as sporadic E tracers, have slopes near 1.1 km/h and 1.8 km/h for the daytime and nighttime sectors respectively, which are in fair agreement with the measured HTI descent rates. It is important to clarify further that the nighttime layer descent rates can be much smaller than the phase velocity of the driving semidiurnal tide, thus one needs to be cautious when using them to compute the vertical tidal wavelength. On the other hand, the descent rates of the morning layer estimated from the HTI ionosonde plots are indeed close to the phase velocity of the diurnal tide.

In summary, the results of this simplified simulation are close to the main observational facts obtained with HTI analysis, e.g., compare the similarity between Figs. 9 and 4. We conclude, that although the present modeling results rely on the very basic wind shear theory and oversimplified assumptions about the wind system, they support at least some aspects of the physical picture and understanding discussed in the previous section.

7. Summary and concluding comments

The main findings of the ionogram HTI analysis of the Milos CADI sporadic E measurements are summarized as follows:

1. The HTI ionogram analysis revealed a semidiurnal periodicity in the formation and altitude descent of sporadic E which dominates most summertime observations. A daytime layer forms at about 120 km near sunrise and descends steadily downward below 100 km by 18 h LT. At about this time a nighttime layer appears above at ~125 km which also moves downward at a somewhat larger descent rate than the daytime layer. From about 16–22 h LT it is possible at times to observe both layers, that is, the daytime below and nighttime above, coexisting.
2. For the summertime observations under consideration, there were time intervals close to solstice when the observed semidiurnal periodicity in sporadic E layer descent and occurrence is weak and a diurnal periodicity becomes predominant. During those times the layers descend at a slower rate near 1.0 km/h. On the other hand, the semidiurnal periodicity prevails clearly after about the end of July as we move toward equinox when E_s becomes gradually weaker. During these times the layers descend faster with rates dz/dt near 1.5 km/h for the daytime layer and 1.9 km/h for the nighttime one.
3. As the sporadic E layers descend with altitude they may disappear and reappear abruptly, sometimes in a periodic-like fashion, but on the average always tend to re-occur near and about the mean slope of altitude descend. In their downward motion, the layers first strengthen in terms of electron density down to about 110 km and then weaken gradually till they become unobservable below about 100 km. This is particularly true for the daytime layer.
4. The HTI analysis reveals at times weak ionosonde traces in the upper E region, that is, at heights above 125–130 km. These upper E region layers appear to occur with a strong semidiurnal,

and at times terdiurnal, periodicity while they descend much faster at rates dz/dt ranging from about 5 to 8 km/h. Also, they appear to connect with, and possibly initiate and/or reinforce, the sporadic E layers that form below 120–125 km.

The key findings of the HTI analysis were interpreted with the aid of using basic wind shear theory and taking into account the forcing effects of the semidiurnal and diurnal tides in the lower thermosphere by assuming an oversimplified wind system. The role of tides is crucial because they provide downward propagating wind shears of ion convergent nodes that form and transport the layers to lower heights. Our study shows that the semidiurnal tide, which dominates over the diurnal tide in the upper E region, plays an important role not only in the formation and transport of the descending intermediate layers but also on the lower E region sporadic E layers, especially during evening and nighttime hours.

We need to stress that the physical picture discussed in this paper is certainly simplified because other factors, which may affect the sporadic E layer formation, were downplayed or ignored. For example, electric field and plasma diffusion effects were not considered as this is a common practice in dealing with mid-latitude sporadic E. Also vertical wind shears in the meridional tidal winds were ignored because at altitudes below 120 km they have a minimal effect; on the other hand, the vertical shears in the zonal wind can be quite effective not only at lower heights but in the upper E region as well. No mention was made of gravity wave effects, which can be important at times in reinforcing or disrupting the tidal forcing of the layers. The most serious omission however has to do with the mechanisms of transport, production and loss of metallic ions, for which there is very little knowledge available. Certainly, the metallic ion lifetimes should be important for obtaining a more thorough understanding of the ionosonde data. For example, the weakening of the layers as they move down below about 110 km should be affected seriously by the anticipated decrease of metallic ion lifetimes with decreasing altitude.

Finally, we have introduced in this paper a new technique for analyzing the ionogram recordings which can help obtain new physical insight into the complex processes of interaction between atmospheric wave dynamics and the ionospheric plasma, particularly with respect to the physics of the plasma-layering phenomena in the upper and lower E region. Although the present HTI ionogram analysis was based on a limited data base, it offered some new hints as how to solve long standing problems on mid-latitude sporadic E, such as, the mystery of the seasonal sporadic E layer morphology that shows a pronounced maximum in the summer and a small maximum in winter. It is hoped to take up this problem in a future study.

Acknowledgments

This work was made possible with the support of: (a) the European Office of Aerospace Research and Development (EOARD), Air Force office of Scientific Research, Air Force Research Laboratory, under contract No FA8655-03-1-3028 to C. Haldoupis, and (b) the Greek Secretariat for Research and Technology and the British Council in Athens through a Greek–British Collaboration Research Grant.

References

Axford, W.I., 1963. The formation and vertical movement of dense ionized layers in the ionosphere due to neutral wind shears. Journal of Geophysical Research 68, 769.

Bishop, R.L., Earle, G.D., 2003. Metallic ion transport associated with midlatitude intermediate layer development. Journal of Geophysical Research 108 (A1), 1019.

Chapman, S., Lindzen, R.S., 1970. Atmospheric Tides. D. Reidel, Hingham, MA.

Chimonas, G., Axford, W.I., 1968. Vertical movement of temperate zone sporadic E layers. Journal of Geophysical Research 73, 111.

Forbes, J.M., 1984. Tidal and planetary waves. In: The Upper Mesosphere and Lower Thermosphere: A Review of Experiment and Theory, vol. 67. American Geophysical Union.

Fujitaka, K., Tohmatsu, T., 1973. A tidal theory of the ionospheric intermediate layer. Journal of Atmospheric and Terrestrial Physics 35, 425.

Haldoupis, C., Pancheva, D., 2002. Planetary waves and midlatitude sporadic E layers: strong experimental evidence for a close relationship. Journal of Geophysical Research 107.

Haldoupis, C., Pancheva, D., Mitchell, N.J., 2004. A study of tidal and planetary wave periodicities present in midlatitude sporadic E layers. Journal of Geophysical Research 109, A02302.

Harper, R.M., 1977. Tidal winds in the 100- to 200-km region at Arecibo. Journal of Geophysical Research 82, 3243.

MacDougall, J.W., 1974. 110 km neutral zonal wind patterns. Planetary and Space Science 22, 545.

MacDougall, J.W., Plane, J.M.C., Jayachandran, P.T., 2000. Polar cap sporadic-E: Part 2, modeling. Journal of Atmospheric and Solar-Terrestrial Physics 62, 1169.

Mathews, J.D., 1998. Sporadic *E*: current views and recent progress. Journal of Atmospheric and Solar-Terrestrial Physics 60, 413.

Mathews, J.D., Bekeny, F.S., 1979. Upper atmospheric tides and the vertical motion of ionospheric sporadic layers at Arecibo. Journal of Geophysical Research 84, 2743.

Pancheva, D., Haldoupis, C., Meek, C.E., Manson, A.H., Mitchell, N.J., 2003. Evidence of a role for modulated atmospheric tides in the dependence of sporadic *E* on planetary waves. Journal of Geophysical Research 108.

Szuszczewicz, E.P., Roble, R.G., Wilkinson, P.J., Hanbaba, R., 1995. Coupling mechanisms in the lower ionospheric–thermospheric system and manifestations in the formation and dynamics of intermediate descending layers. Journal of Atmospheric and Terrestrial Physics 57, 1483.

Tong, Y., Mathews, J.D., Ying, W.-P., 1988. An upper *E* region quarterdiurnal tide at Arecibo? Journal of Geophysical Research 93, 10,047.

Whitehead, J.D., 1989. Recent work on mid-latitude and equatorial sporadic-*E*. Journal of Atmospheric and Terrestrial Physics 51, 401.

Wilkinson, P.J., Szuszczewicz, E.P., Roble, R.G., 1992. Measurements and modeling of intermediate, descending, and sporadic layers in the lower ionosphere: results and implications for global-scale ionospheric–thermospheric studies. Geophysical Research Letters 19, 95.